Highly sensitive strain detection in silicon by reflectance anisotropy spectroscopy

D. Papadimitriou[1] and W. Richter[2]
[1]*National Technical University of Athens, Department of Physics, GR-15780 Athens, Greece*
[2]*Technical University of Berlin, Institute of Solid State Physics, Hardenbergstr. 36, D-10623 Berlin, Germany*
(Received 3 March 2005; published 29 August 2005)

Reflectance anisotropy spectroscopy (RAS) measurements were performed on strained silicon (Si) stripes cut from crystalline silicon wafers. Strains were externally applied using a device developed especially for the study of layers and layered structures. The dependence of the RAS signal intensity on strain was measured for (100), (110), and (111) silicon wafers strained along [001] and [011]. In these configurations, the RAS spectra show a derivativelike structure at 3.4 eV, which increases in amplitude linearly with strain. While RAS line shapes depend on the orientation of the Si wafer and the crystallographic directions along which strains are applied, RAS intensities depend on strain magnitude. Strains as low as 10^{-5} can be measured, which is two orders of magnitude smaller than those detected with standard techniques such as Raman, piezoelectroreflectance spectroscopy (PERS), or x-ray diffraction (XRD). The experimental RAS spectra are found to be in good agreement with spectra calculated on the basis of the spectral response of the published piezo-optical tensor components. It is concluded that RAS provides a highly sensitive tool for the detection of strain induced bulk anisotropies. Strain calibrated RAS spectra can be used for strain-stress characterization of semiconductor layers and microstructures with a higher efficiency than that achieved by Raman, PERS, and XRD. Combined with growth techniques, RAS spectroscopy can be also used for *in situ* control of strain during semiconductor growth.

DOI: 10.1103/PhysRevB.72.075212 PACS number(s): 78.20.Hp, 78.40.Fy

INTRODUCTION

Numerous diagnostic procedures have been employed in the past for strain/stress characterization of semiconductor samples, the most pronounced example being the optical techniques. They are nondestructive and offer the possibility of *in situ* applications. Raman spectroscopy, a well established experimental tool, is based on the detection of strain induced phonon frequency shifts.[1] Piezoelectroreflectance and piezophotoreflectance spectroscopy, on the other hand, are applied to investigate the effect of strain on the electronic bands.[2] These methods can detect strains in the range of 10^{-3}, which, however, is not sufficient in many applications. Because of this low sensitivity, with the kind of piezodevices used in the past,[2,3] the samples had to be cut into small highly polished rods of about $2\times2\times20$ mm in order to obtain sufficiently high uniaxial stresses that can be detected with the optical spectroscopic techniques referred to above. This made studies on thin solid films, heterostructures, and superlattices, which have become in recent years the main aspect of device materials and related technologies, almost impossible.

In previous published works,[4,5] a device was developed and used for externally controlled application of strain on thin layers. It was shown, then, that strains in thin layers can be detected by means of Raman and reflectance anisotropy spectroscopy (RAS). In addition RAS provided a much higher sensitivity and thus promised to be suitable for the detection of very small amounts of strain.

In the present work, extensive studies on strained silicon stripes cut along various crystallographic directions were performed and the dependence of intensities, energies, and line shapes of the reflectance anisotropy of bulk silicon on externally applied strain was measured in various configurations (Table I) with the aim of using strain calibrated RAS spectra for strain characterization during *in situ* and *ex situ* studies of layered structures. Under the application of strain/stress, sharp optical resonances have been observed at the critical points of the bulk dielectric function.[2] Strain-dependent features are found to develop in the RAS spectra already at strains as low as 10^{-5} and can be conveniently measured for strains in the range of 10^{-4} or higher. This is a sensitivity two orders of magnitude higher than that of other spectroscopic methods such as Raman, PERS, and XRD. Thus, RAS has proved to be almost a unique tool for strain/stress characterization.

Some RAS spectra on strained Si(001), Si(110), and Si(111) surfaces have already been discussed in Refs. 6 and 7. However, there, measurements were performed not with the purpose of an accurate quantitative strain calibration, but

TABLE I. Crystallographic configurations of the silicon stripes measured.

	Si surface z axis	Reflectance anisotropy $\Delta R=r_x-r_y$	Strain e_x
1	(100)	$r_{010}-r_{001}$	$e_x//[010]$
2		$r_{010}-r_{001}$	$e_x//[001]$
3		$r_{011}-r_{0\bar{1}1}$	$e_x//[011]$
4		$r_{011}-r_{0\bar{1}1}$	$e_x//[0\bar{1}1]$
5	(110)	$r_{\bar{1}10}-r_{001}$	$e_x//[001]$
6		$r_{\bar{1}10}-r_{001}$	$e_x//[\bar{1}10]$
7		$r_{\bar{1}11}-r_{\bar{1}1\bar{2}}$	$e_x//[\bar{1}11]$
8	(111)	$r_{\bar{1}10}-r_{11\bar{2}}$	$e_x//[\bar{1}10]$

 ©2005 The American Physical Society

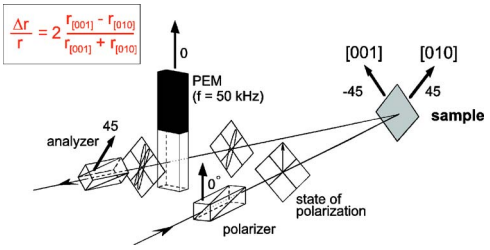

FIG. 1. (Color online) Beam path in the RAS spectrometer: the sample is adjusted with its strain axis under 45° to the polarizer and PEM axis.

for the purpose of qualitatively correlating optical effects with stresses induced by the formation of dimers on the sample surface. Moreover, no derivation of the equations relating the change of the dielectric function to the applied stress was given. In addition, the notation of the stress components was not standard and could be easily misunderstood.

Taking all these in account, the aims of the present work are (1) to extend previously performed studies on uniaxially stressed bulk crystals[2,3] to strain studies of layered structures which are the basis of modern device technology, (2) to calibrate very small, but for device applications still critical, amounts of strain ($\leqslant 10^{-4}$) by applying RAS as *in situ* and *ex situ* strain detection method, and (3) to elaborate a clear formalism in order to calculate the optical response of strained layers in several configurations, a problem, in principle known, but not trivial.

EXPERIMENT

Silicon stripes of 20 mm length and various widths, ranging from 3 to 10 mm, were cut from silicon (100), (110), and (111) wafers of 0.3–0.6 mm thickness. They were cleaved (or sawed) along low index crystallographic directions. In Table I, all the configurations used are listed. The stripes were etched with HF according to Ref. 8. By etching, the amorphous SiO_2, formed on the Si surface by exposure in air, is completely removed. However, the freshly etched surface is relatively quickly covered by a new oxide layer, so that no significant differences could be found between the RAS spectra recorded within the first hour and many hours later.

Strains were applied along one of the main crystallographic axes of the sample (defined as the x axis) and the differences of the reflectance components parallel and perpendicular to the strain axis were detected simultaneously using RAS. The experimental setup (Fig. 1) was similar to that described in Ref. 9. The ac signal was generated by a photoelastic modulator (PEM) operated at 50 kHz. The PEM was adjusted with its axis under 45° to the direction of strain (Fig. 1). For a sample in the (xy) plane, the detected RAS signal is given by

$$\frac{\Delta r}{\bar{r}} = \frac{2(r_x - r_y)}{(r_x + r_y)}, \tag{1}$$

$\Delta r = r_x - r_y$ being the difference of the reflectance amplitude coefficients along the x and y axis of the sample surface. This

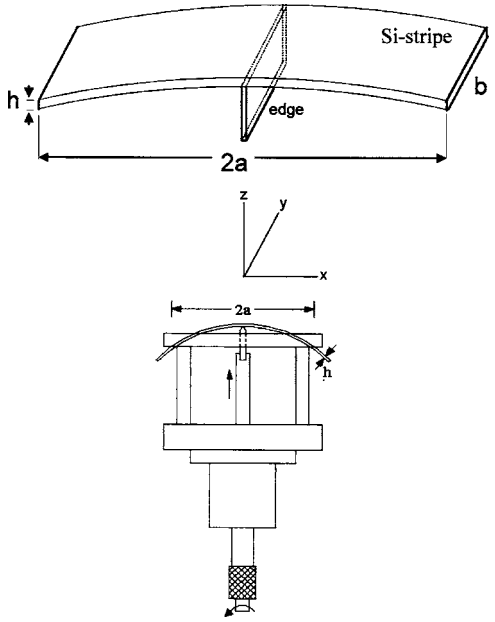

FIG. 2. Schematic drawing of a silicon stripe under strain induced by the movement of a sharp edge in the direction of the z-axis (stripe curvature enlarged by a factor of 10^3).

difference is normalized to the average of the amplitude coefficients of the sample $\bar{r} = 1/2(r_x + r_y)$, resulting in a quantity independent of fluctuations in the intensity of the light source and of the electronic signal. The RAS signal $\Delta r/\bar{r}$ is, therefore, proportional to the ac/dc ratio, which is of the order 10^{-3}. RAS spectra were measured in the range 1.5–5.5 eV.

As shown in Fig. 2, strains were induced by the application of a line force at the center of the stripe using the device introduced in Ref. 5: An edge positioned in the middle of a stripe of length ($2a$), parallel to the stripe short side (b), is moving by a micrometric screw against the surface of the stripe that is supported at its ends. Long and short sides of the stripe are directed along the x and y axis, respectively, while the edge moves in the direction of the z axis. For deformations smaller than the thickness of the stripe, the strain along the long side of the stripe depends on the deformation $J(r)$, where r is the distance from the center of the stripe.[10,11] The maximum strain e_0, at the center, can be calculated, independently of material elasticity, from the stripe dimensions and the measured central deformation J_0 as

$$e_x = e_0 = \frac{3hJ_0}{2a^2}, \tag{2}$$

where $2a$ and h are the length and the thickness of the stripe, respectively, and J_0 is the deformation at the center which is given directly by the movement of the micrometric screw.[5] In addition, the maximum strain e_0 can be calculated by measuring the radius of curvature of the bent stripe with a laser beam deflection method as suggested in Ref. 4. The results obtained for the strain from Eq. (2) and by the beam deflection method[4] were consistent within the experimental error (5%).

The strain device, which is also the sample (=stripe) holder, was mounted on a table that could be rotated allowing for optical alignment. The sample was adjusted with its strain axis under 45° to the polarizer and PEM axis of the RAS spectrometer (Fig. 1). This configuration enables simultaneous measurement of the reflectance amplitude coefficients parallel and perpendicular to the applied strain in accordance with Eq. (1). Sample adjustment was achieved by application of an initial strain and rotation to the position of zero RAS signal. At this position, the strain axis is oriented along the polarizer axis. For each strain value, RAS spectra were recorded at 45° and 135° (45°+90°) angle of strain axis to polarizer axis. In this way, the polarization influence of optical components on the sample reflectance can be eliminated.

Several control experiments were performed. Samples were measured twice with the strain applied along each one of the cleaved faces. Sets of measurements along equivalent directions of strain (e.g., [010] and [001] or [011] and $[0\bar{1}1]$ directions of the Si (100) surface) gave identical RAS spectra. RAS spectra were also recorded from different regions of the sample surface and showed no differences. This proves experimentally that the stripe is homogeneously bent (that is, the radius of curvature over the stripe area is constant) consistent with theoretical predictions.[10]

THEORETICAL CONSIDERATIONS

The introduction of a homogenous strain in a solid produces changes in the lattice parameter and the symmetry of the material. These in turn produce significant changes in the electronic band structure and in the vibrational modes. All configurations of homogenous strain consist of an isotropic (or hydrostatic) and an anisotropic component. The first gives rise to a volume change without disturbing the crystal symmetry, while the latter, in general, reduces the symmetry present in the strain-free lattice. Changes in energy gaps, splittings due to the lowering of symmetry, and variations in effective masses occur.

Without strain or spin-orbit splitting, the valence-band edge at $k=0$ in a diamond- or zinc blende–type material is a sixfold degenerate multiplet with orbital symmetry $\Gamma_{25'}$ (diamond) or Γ_{15} (zinc blende).[2] The spin-orbit interaction lifts this degeneracy into a fourfold $p_{3/2}$ multiplet ($J=3/2$, $m_J=\pm 3/2, \pm 1/2$) and a $p_{1/2}$ multiplet ($J=1/2$, $m_J=\pm 1/2$). The application of an uniaxial stress splits further the $p_{3/2}$ multiplet and also, because of the hydrostatic pressure component of the strain, shifts the $p_{3/2}$ and the $p_{1/2}$ bands relative to the conduction band.[2] A detailed analysis of Δ transitions near $\Gamma(k\neq 0)$ is considered to be difficult[2] since the Δ_2 valence band states are strongly mixed into Δ_5 by the spin-orbit interaction. This interaction is usually neglected in considerations of the interband transitions in Si since spin-orbit splittings in this material are small ($\Delta_0=0.044$ eV, $\Delta_0' \approx 0.025$ eV) compared with the direct gaps. However, the application of an uniaxial stress would change the spin-orbit splitting of the orbital valence bands; it would produce, in termini of Ref. 2, an orbital intraband stress splitting, meaning that it would shift already split bands[2] or that it would split and shift non spin-orbit split bands. Dependent on stress magnitude, this might be of the same order as the spin-orbit splitting itself, so that both interband and intraband splitting of Δ transitions have to be considered.

Cubic materials, such as silicon, are known to be optically isotropic. Lowering the symmetry by the application of an external force produces optical bulk anisotropy, which can be sensed very effectively by RAS. Dependent on the direction of applied strain, the band structure of the material is modified, degeneracies are removed, and sharp peaks appear in the RAS spectrum at transition energies near the critical points. The transition energies of the unstrained Si lattice are given as follows:[12] $E_0=4.185$ eV, $E_0+\Delta_0=4.229$ eV, $E_1=3.45$ eV, $E_0'=3.378$ eV, and $E_2=4.33$ eV, $E_1'=5.50$ eV, where E_0 and E_1, E_0', E_2, E_1' are the fundamental and higher gap energies of Si, respectively, and Δ_0 is the energy due to the spin-orbit interaction. These values will be used in the discussion of the RAS spectra.

The observed reflectance anisotropies are due to the difference of the reflectance changes along the in-plane crystallographic axes of the sample by application of strain/stress along one of these axes. These reflectance changes are directly related to the changes in the dielectric function of the bulk.

In the next section, the changes in the dielectric function of silicon will be calculated in dependence of the piezo-optical effects induced by the application of strain/stress. Strains/stresses are given in the Appendix in dependence of the experimental parameters (J_0, $2a$, h) and the material properties of silicon (elastic compliances S_{ij}) for all configurations of the strained Si stripes. In the Results and Discussion section, the calculated reflectance anisotropy spectra are compared to the measured spectra.

Determination of strain/stress-induced changes in the dielectric function and the reflectivity. The optical properties of crystals are described, in general, by symmetric second-rank tensors $n_{ij}(\omega)$ and $\kappa_{ij}(\omega)$ (refractive index and absorption coefficient), or $\varepsilon_{1\,ij}(\omega)$ and $\varepsilon_{2\,ij}(\omega)$ (real and imaginary parts of the dielectric function ε_{ij}).[13] The reflectivity R and several other optical functions are related to $\varepsilon_1(\omega)$ and $\varepsilon_2(\omega)$. The effects of a stress or a strain on the dielectric function $\varepsilon(\omega)$ of a crystal are represented by a fourth rank tensor, called the piezo-optical or stress-optical tensor P_{ijkl}, which connects the components of the stress-induced changes in the dielectric function $\Delta\varepsilon(\omega)$ with those of the applied stress tensor X as follows[13,14]:

$$\Delta\varepsilon_{ij}(\omega) = P_{ijkl}(\omega)X_{kl}. \tag{3}$$

The piezo-optical tensor of amorphous and most cubic solids (those with point group O_h, O, and T_d) has only three independent components, P_{1111}, P_{1122}, and P_{1212}, which in supressed-index notation[15] are labeled as P_{11}, P_{12}, and $P_{44}/2$, respectively. A change in the dielectric function induces a change in the reflectivity given by[13]

$$\frac{\Delta[R(\omega)]}{R(\omega)} = \alpha\Delta\{\mathrm{Re}[\varepsilon(\omega)]\} + \beta\Delta\{\mathrm{Im}[\varepsilon(\omega)]\}, \tag{4}$$

where α and β are the Seraphin coefficients,[16] which determine to what extend changes in the real and imaginary parts

of the dielectric function contribute to the change in reflectivity $\Delta R/R$. By using the $P_{11}(\omega)$, $P_{12}(\omega)$, and $P_{44}(\omega)$ components of P_{ijkl} obtained in Ref. 17, the difference of the stress-induced changes in the reflectivity components along the two optical axis of the sample surface can be calculated according to Eqs. (3) and (4). The calculated spectra can then be directly compared to the measured reflectance anisotropy spectra of the strained layers.

Alternatively, reflectance differences for bulk processes can be described using the basic equation of modulation spectroscopy as suggested in Ref. 18:

$$\frac{R_x - R_y}{R} = \mathrm{Re}\left[\frac{2n_\alpha(\varepsilon_{xx} - \varepsilon_{yy})}{n_s(\varepsilon_s - \varepsilon_\alpha)}\right], \tag{5}$$

where ε_{xx} and ε_{yy} are the components of the dielectric tensor along the crystallographic axis x and y, respectively, ε_s and $n_s = \sqrt{\varepsilon_s}$ are the average dielectric function and the refractive index of the bulk, and n_α is the index of refraction of the ambient. For $n_\alpha = 1$ (air) and nonzero absorption $\varepsilon = \varepsilon_1 + i\varepsilon_2$, Eq. (5) can be written as

$$\frac{\Delta R}{R} = \frac{\Delta\varepsilon}{(\varepsilon - 1)\sqrt{\varepsilon}}. \tag{6}$$

According to Eq. (6), changes in reflectance can be calculated from the dielectric function, measured by spectroscopic ellipsometry,[19] and the changes in dielectric function, as given below, without reference to the Seraphin coefficients.

In the following, we will use both approaches [Eqs. (4) and (6)]; a comparison can be found in Fig. 5.

The strain induced changes in the dielectric function of silicon (investigated in the configurations listed in Table I) under the assumption of a biaxial stress in the x-y plane [as defined by Eq. (A6) in the Appendix] and light propagation along the z axis, are as follows.

For a Si(100) surface in the configuration No. 1 or 2 ([010], [001], [100]), the changes in the dielectric function $\Delta\varepsilon$, in terms of the applied stresses X_x, X_y are

$$\Delta\varepsilon = (P_{11} - P_{12})(X_x - X_y). \tag{7a}$$

The in-plane stress defined in Eq. (7a) can be converted to strain with the help of Eq. (A6) and $\Delta\varepsilon$ can be expressed in dependence of the applied strain e_x:

$$\Delta\varepsilon = (P_{11} - P_{12})\left(\frac{e_x}{S_{11} - S_{12}}\right). \tag{7b}$$

For a Si(100) surface in the configuration No. 3 or 4 ([$0\bar{1}1$], [011], [100]):

$$\Delta\varepsilon = P_{44}(X_x - X_y), \tag{8a}$$

$$\Delta\varepsilon = P_{44}\left(\frac{e_x}{S_{11} - S_{12}}\right). \tag{8b}$$

For a Si(110) surface in the configuration No. 5 ([001], [$\bar{1}$10], [110]):

$$\Delta\varepsilon = (P_{11} - P_{12})X_x + \frac{(P_{12} - P_{11} - P_{44})}{2}X_y, \tag{9a}$$

$$\Delta\varepsilon = \left[\frac{(2S_{11} + S_{12})(P_{11} - P_{12}) + S_{12}P_{44}}{2}\right]\left(\frac{e_x}{S_{11}^2 - S_{12}^2}\right). \tag{9b}$$

For a Si(110) surface in the configuration No. 6 ([$\bar{1}$11],[$\bar{1}1\bar{2}$], [110]):

$$\Delta\varepsilon = P_{44}X_x + \frac{(P_{12} - P_{11} - 5P_{44})}{6}X_y, \tag{10a}$$

$$\Delta\varepsilon = \left[\frac{S_{12}P_{11} - S_{12}P_{12} + (6S_{11} + 5S_{12})}{6}\right]\left(\frac{e_x}{S_{11}^2 - S_{12}^2}\right). \tag{10b}$$

Configuration No. 7 ([$\bar{1}$11],[$\bar{1}1\bar{2}$], [110]) of the Si(110) surface is not considered here, because application of strain along the [$\bar{1}$11] crystallographic axis (e_x//[$\bar{1}$11]) did not gave RAS spectra with significant changes in the reflectance difference and was not evaluated. For a Si(111) surface in the configuration No. **8** ([$11\bar{2}$],[$\bar{1}$10], [111]):

$$\Delta\varepsilon = (X_x - X_y)\frac{(P_{11} - P_{12} + 2P_{44})}{3}, \tag{11a}$$

$$\Delta\varepsilon = \left(\frac{P_{11} - P_{12} + 2P_{44}}{3}\right)\left(\frac{e_x}{S_{11} - S_{12}}\right). \tag{11b}$$

Equation (7a) results directly from the multiplication of the piezo-optical tensor of cubic crystals given in Ref. 15 with the stress tensor describing an in-plane stress (biaxial stress), while Eqs. (8a), (9a), (10a), and (11a) are deduced by transformation of the piezo-optical tensor in the respective configuration according to the method introduced in Ref. 20 and briefly discussed in the Appendix. Equations (7b), (8b), (9b), (10b), and (11b) are equivalent to Eqs. (7a), (8a), (9a), (10a), and (11a), but changes in the dielectric function are related, through Eq. (A6) of Appendix, to the experimentally induced strain and the elastic compliances of silicon. In Eqs. (7a), (8a), and (11a), the first term, which is a linear combination of the piezo-optical tensor components, describes the spectral distribution of RAS-intensities, while the second term, which is related to the applied stress, is actually a constant factor modifying only the strength of the RAS intensities. On the contrary, in Eqs. (9a) and (10a), RAS intensities and line shapes are determined by a mixing of stress and piezo-optical-tensor components. For the isotropic silicon surfaces, Si(100) and Si(111), the externally applied strains are, thereafter, responsible only for the observed intensity changes of the RAS spectrum, whereas RAS energies and line shapes are described by the components of the piezo-optical tensor. For the anisotropic silicon surface Si(110) transition energies, line shapes, and intensities as well are dependent on both the piezo-optical tensor components and the applied strain.

In the following, the experimental RAS spectra will be compared to spectra calculated according to Eq. (4) [or Eq. (6)] with the strain induced changes of the dielectric function obtained from Eqs. (7b), (8b), (9b), (10b), and (11b).

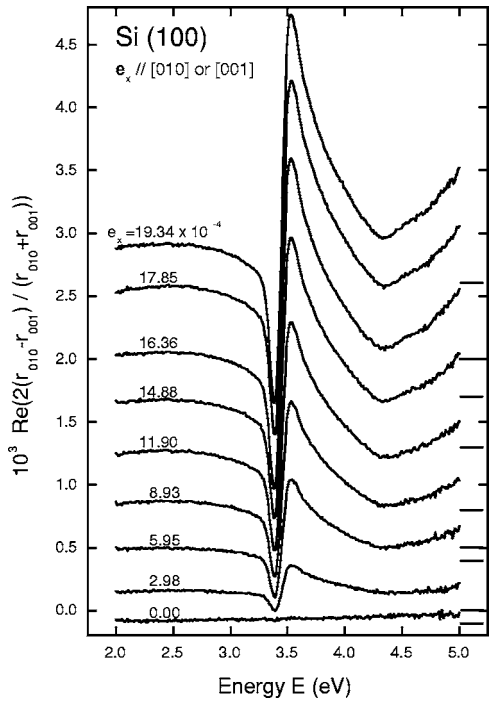

FIG. 3. Spectra of reflectance anisotropy $(r_{010}-r_{001})$ of Si(100) stripes strained along [010] or [001] (for clarity, spectra are shifted in $\Delta r/\bar{r}$; zero strain lines are indicated).

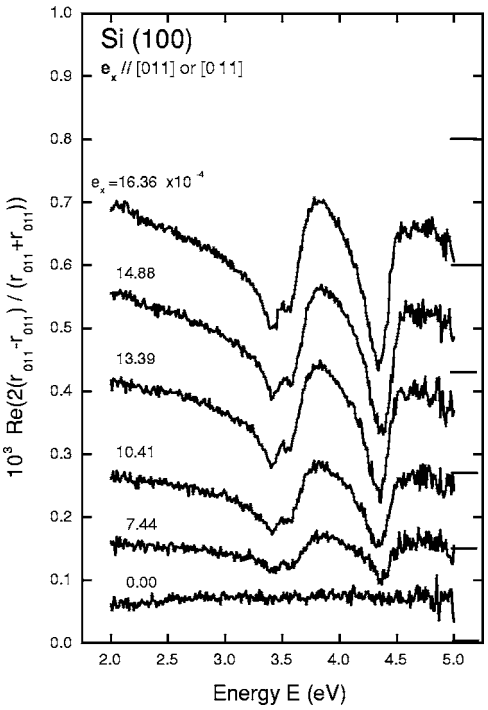

FIG. 4. Spectra of reflectance anisotropy $(r_{011}-r_{0\bar{1}1})$ of Si(100) stripes strained along [011] or $[0\bar{1}1]$ (for clarity, spectra are shifted in $\Delta r/\bar{r}$; zero strain lines are indicated).

RESULTS AND DISCUSSION

A. Silicon (100) surface

The reflectance differences along the [010] and [001] (configurations Nos. 1 and 2 in Table I) or along the [011] and $[0\bar{1}1]$ directions of Si(100) stripes (configurations Nos. 3 and 4 in Table I) are presented in Figs. 3 and 4, respectively. Since the oxidized (100) Si surface is highly isotropic, it has no contribution to the observed optical anisotropy. Without the strain induced bulk anisotropy, the RAS signal of unstrained stripes is zero as expected for an oxygen (or hydrogen) passivated unreconstructed Si surface. (We remind the reader that the Si stripes studied here were used either directly, without removal of the SiO_2, or they were etched with HF, which made no difference in the RAS spectra). Though in recent publications,[6,7] some of the features observed on the optical data of Si surfaces have been associated with strain effects induced by surface reconstruction, steps or dimerization, it should be pointed out that dimer formation and surface reconstruction involve UHV-clean Si-surfaces as reported in Ref. 21. Consequently, the RAS signal of a nonmiscut Si(100) or Si(111) surface is zero as shown in the present work and in Ref. 6.

Under the influence of a strain along [010], the RAS spectra of the stripes (Fig. 3) show the development of a sharp peak at 3.39 eV (E_0') and a broad band at 4.34 eV (E_2). In the spectra of stripes strained along [011], the 3.39 eV peak is broadened and separated into two peaks at 3.34 and 3.49 eV (E_0', E_1), while the 4.34 eV band is sufficiently narrowed (Fig. 4). Similar splittings were observed in the E_0' peaks of the piezoelectroreflectance spectra of Si rods[2] under uniaxial stresses along [001] or [110] and were interpreted as indicative of $\Delta_5-\Delta_1$ (E_0') interband transitions between the upper valence band Δ_5 and lower conduction band Δ_1. Intraband splitting of the Δ_5 valence band,[2] as described in the Theoretical Considerations section, as well as stress-induced intraband coupling of Δ_1 to Δ_2 (Ref. 22) have then to be taken into account. For [010] or [001] strains, the RAS-peak intensity is at least one order of magnitude higher than that for [011] or $[0\bar{1}1]$ strains (Figs. 3 and 4). The sensitivity of optical response in the configuration No. 1 or 2 ([100], [010], [001]) in comparison with the configuration No. 3 or 4 ([100], [011], $[0\bar{1}1]$) may indicate a larger deformations potential in the first case.

In Fig. 5, the experimentally observed RAS spectra for [011] or $[0\bar{1}1]$ strain [Fig. 5(a)] are compared to the spectra calculated from the piezo-optical tensor components[17] using Eqs. (4) and (8b) [Fig. 5(b)] or Eqs. (6) and (8b) [Fig. 5(c)] The experimental line shapes (e.g., the W shape of the 3.39 eV band and the distinct 4.34 eV band) are, in case of [011] strain, and almost in case of $[0\bar{1}1]$ strain, well reproduced by the calculation. However, both theoretically calculated spectra are shifted by 100–120 meV to lower energies with respect to the measured spectrum. A similar energy shift appears also by comparison of experimental and calculated spectra for [010] or [001] strain (Fig. 6). In this case, Eqs. (4) and (7b) were used to calculate the RAS spectrum. Though an almost linearly increasing background is superimposed to the calculated spectrum [Fig. 6(b)], the spectral structures at 3.39 and 4.34 eV can be compared to the experimental RAS bands [Fig. 6(a)]. In general, energy shifts observed in the

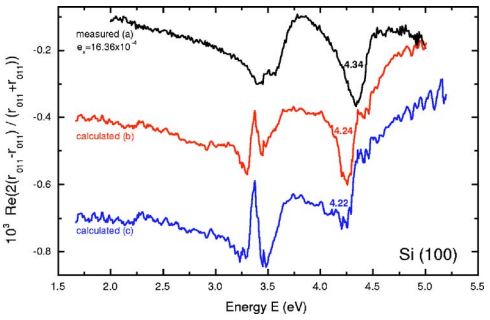

FIG. 5. (Color online) Comparison of (a) the experimentally measured reflectance anisotropy $(r_{011}-r_{0\bar{1}1})$ of the Si(100) surface strained along [011] or $[0\bar{1}1]$ with the reflectance anisotropy calculated from the piezo-optical tensor components (Ref. 17) according to (b) Eqs. (4) and (8b), and (c) Eqs. (6) and (8b).

optical spectra may be associated with the oxide coverage of the sample surface, then in accordance with Eqs. (4)–(6) an effective dielectric function, including that of the surface oxide, is measured. Thus, the energy discrepancies between our calculated and measured RAS spectra very probably result from differences in the surface coverage of our samples to the samples studied in Ref. 17.

For strain calibration, the RAS intensities measured from peak minimum to peak maximum were used. In both configurations Nos. 1 or 2 ([100], [010], [001]) and Nos. 3 or 4 ([100], [011], $[0\bar{1}1]$) of Si(100), the intensity $\Delta r/\bar{r}=2(r_{010}-r_{001})/(r_{010}+r_{001})$ of the 3.39 eV peak, measured from peak minimum at 3.39 eV to peak maximum at 3.53 eV, and also the intensity $\Delta r/\bar{r}=2(r_{011}-r_{0\bar{1}1})/(r_{011}+r_{0\bar{1}1})$ of the double peak at 3.34 and 3.49 eV vary linearly with the applied strain as calculated by the central deformation of the stripe [Eq. (2)]. This dependence is shown for [010] and [001] strains in Fig. 7 (solid line).

We note that in the present measurements on Si (100) stripes (Fig. 7, full squares), the slope of $\Delta r/\bar{r}$ in dependence of applied strain e is by factor 3 smaller than that reported in previously published measurements.[5] There, however, silicon wafers with 10° miscut from the (001) plane were used, which can produce additionally optical anisotropy.[6] Thus our present data represent a more accurate result for Si(100).

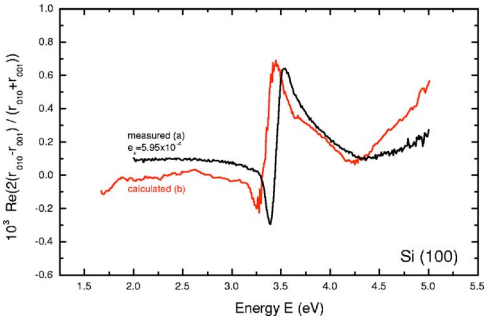

FIG. 6. (Color online) Comparison between (a) the experimentally measured reflectance anisotropy $(r_{010}-r_{001})$ of the Si(100) surface strained along [010] or [001] and (b) the reflectance anisotropy calculated from the piezo-optical tensor components (Ref. 17) according to Eqs. (4) and (7b).

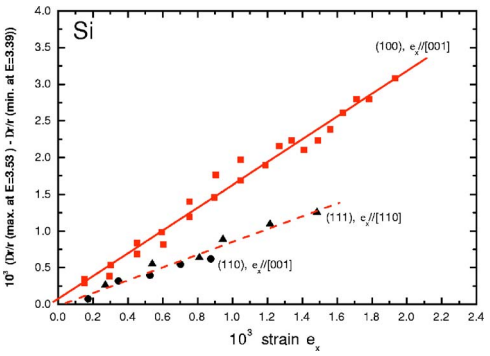

FIG. 7. (Color online) Dependence of the RAS-signal intensity on applied strain in the following configurations: reflectance anisotropy $(r_{010}-r_{001})$ of Si(100) stripes strained along [010] or [001] (■, solid line), reflectance anisotropy $(r_{\bar{1}10}-r_{001})$ of Si(110) stripes strained along [001] (●, dashed line), reflectance anisotropy $(r_{\bar{1}10}-r_{11\bar{2}})$ of Si(111) stripes strained along $[\bar{1}10]$ (▲, dashed line).

B. Silicon (110) surface

In Fig. 8 the RAS spectra of the strained and unstrained silicon (110) surface, which is optically anisotropic, are shown. For a clean surface of a cubic semiconductor, an important contribution to the RAS signal comes from surface states and surface reconstruction.[23] In the case of oxygen (or hydrogen) passivated unreconstructed Si(110) surface [natural Si(110)], the reflectance anisotropy may arise, as recently shown,[24] from intrinsic anisotropy and surface local-field effects, both closely connected to surface roughness and the

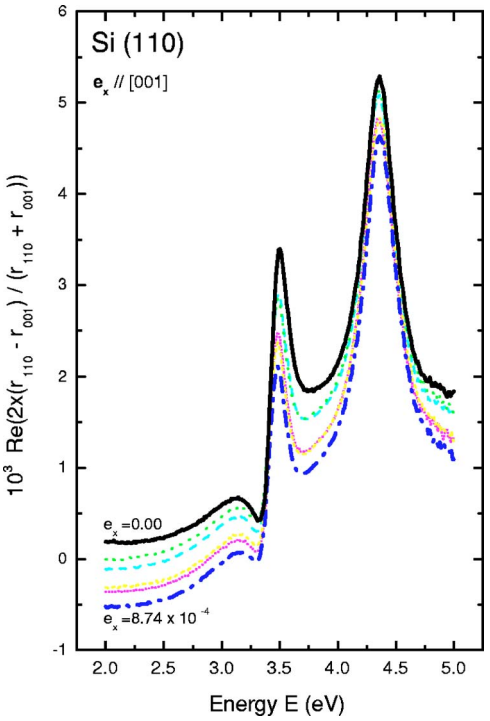

FIG. 8. (Color online) Reflectance anisotropy spectra $(r_{\bar{1}10}-r_{001})$ of the strained and unstrained Si(110) surface, which is optically anisotropic [strains are varied between $e_x=0$ (solid line) and $e_x=8.74\times10^{-4}$ (dot-dashed line), see also Fig. 9].

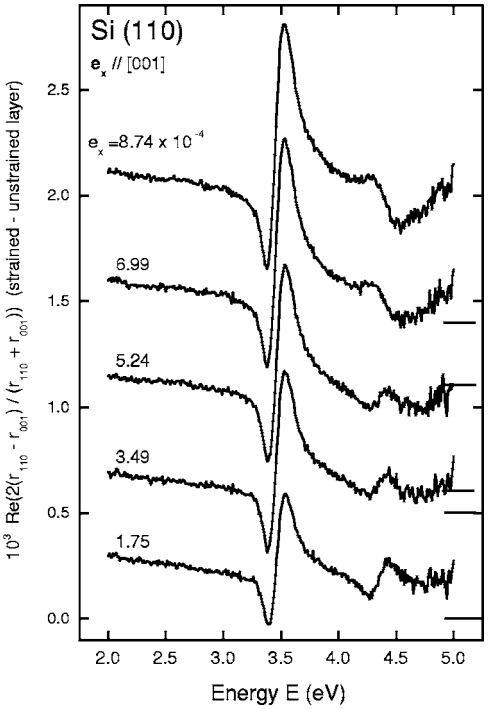

FIG. 9. Spectra of reflectance anisotropy ($r_{\bar{1}10}-r_{001}$) of Si(110) stripes strained along [$\bar{1}$10] after subtraction of the spectrum of the unstrained stripe (for clarity, spectra are shifted in $\Delta r/\bar{r}$ of the spectrum at strain $e_x=1.75\times10^{-4}$; zero strain lines are indicated).

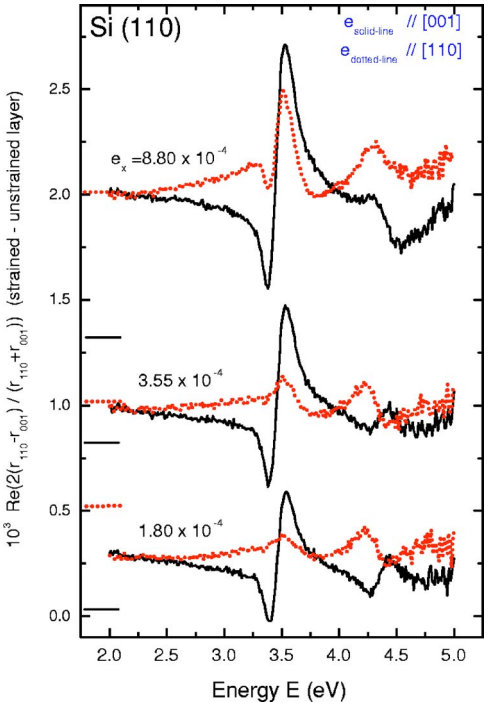

FIG. 10. (Color online) Comparison of RAS spectra ($r_{\bar{1}10}-r_{001}$) of the Si(110) surface strained along [$\bar{1}$10] (dotted line) and [001] (solid line).

presence of atomic defects. Under the application of strain, degeneracy removal and upper-valence band lifting are additionally observed, as already stated above, and give rise to an enhancement of the optical anisotropy. By the study of an anisotropic Si(110) surface, therefore, the spectra of the strain-free samples have to be subtracted from the spectra of the strained samples in order to separate the strain-induced anisotropy from the intrinsic anisotropy and the anisotropy related to surface-field effects.

Strains were applied along the [111] direction in the configuration ([110], [$\bar{1}$11],[$\bar{1}\bar{1}$2], No. 7 in Table I) and along both the [$\bar{1}$10] and the [001] directions in the configuration ([110], [$\bar{1}$10], [001], Nos. 6 and 5 in Table I) (Figs 8, 9, and 10). In the first case (No. 7), no significant changes could be observed between the spectra of strained and unstrained layers. Maximum changes were observed with increasing strain on the spectra of stripes strained along [001] (Fig. 8). After subtraction of the spectrum of the unstrained from the spectra of the strained stripes (Fig. 9), spectral features similar to those already observed on the RAS spectra of Si(100) at 3.39 and 4.34 eV (Fig. 3), could be recognized. In addition, a splitting of the broad band at 4.34 eV into two bands at 4.27 and 4.54 eV occurred, as can be seen by comparison of the spectra of Si(100) and Si(110) strained along [001] (Figs. 3 and 9). In these configurations the (100) and (110) stripes exhibit in all directions strains equal to one another [Eq. (A8)], but their optical response is different [Eq. (1)]. At strain values of about 2×10^{-4} both bands have comparable intensities. With increasing strain, the intensity of the 4.27 eV band decreases in favor of the band at 4.54 eV and disappears at strain values lower than 10^{-3}.

The RAS line shapes of Si(110) stripes at equal strain values along the [$\bar{1}$10] and [001] directions (Fig. 10) indicate that band deformation with increasing strain may proceed faster for [001] than for [$\bar{1}$10] strains. RAS intensities at 1.8×10^{-4} [001] strain are almost comparable with those at 8.8×10^{-4} [$\bar{1}$10] strain (Fig. 10). Thus, loads along [001] and equivalent directions can be sensored by RAS very effectively.

In Fig. 11, a measured RAS spectrum of Si(110) strained along [001] in the configuration ([110], [$\bar{1}$10], [001]) is compared with RAS spectra calculated according to Eqs. (4) and (9b) by using the piezo-optical tensor components of Ref. 17.

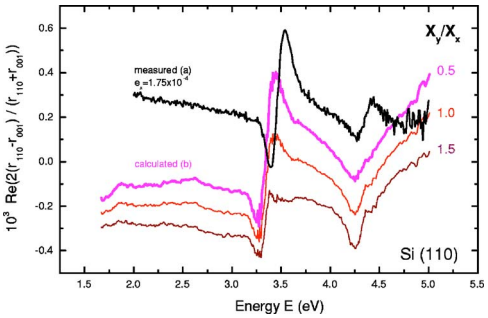

FIG. 11. (Color online) Comparison between (a) the experimentally measured reflectance anisotropy ($r_{\bar{1}10}-r_{001}$) of the Si(110) surface strained along [001] and (b) the reflectance anisotropy calculated from the piezo-optical tensor components (Ref. 17) according to Eqs. (4) and (9b) for three different ratios (0.5, 1, and 1.5) of the components X_y/X_x of a biaxial stress in the xy plane.

In case of an anisotropic Si(110) surface, not only the intensities, but also the energies and line shapes of the RAS spectra are affected by the applied strain/stress, as discussed in the section of the theoretical considerations. This effect is demonstrated in Fig. 11 by simulating the RAS spectra for a biaxial stress X in the xy plane with a component ratio of X_y/X_x of 0.5, 1, and 1.5. As can be seen by comparison of the measured [Fig. 11(a)] and the simulated spectra [Fig. 11(b)], the best fit to the experimental data is given by $X_y=0.5\ X_x$. The inability to reproduce the energy positions of the RAS peaks and the splitting of the RAS band at 4.34 eV (E_2 energy gap) in the simulated spectra could possibly result from the influence of the surface coverage of the samples investigated in Ref. 17 to the presently measured samples. In the case of an oxide coverage, its thickness may increase during the measurements and influence the differences of the spectra of the strained to the unstrained samples. The fact that (a) the thickness of the surface oxide, defined at the beginning of the measurement, may change during the measurement, and that (b) strains determine both RAS intensities and RAS energies and line shapes, makes it, generally, difficult to simulate the spectra of an anisotropic Si(110) surface.

The derivativelike structure at 3.39 eV in the RAS spectra of Fig. 9 was evaluated the same way as for the Si(100) stripes and the results are presented in Fig. 7 together with those of measurements on Si(100) and Si(111) stripes. Although the linearity is evident, there was still a remaining signal in the evaluated spectra of $\Delta r/\bar{r}=0.5\times10^{-3}$ at strain values zero. This may be due to the fact, that the unstrained state cannot be determined in the case of anisotropic surfaces with equal certainty as in the case of isotropic surfaces, which at zero strain have no RAS signal. The estimated values were renormalized to give zero RAS signal at zero strain before they were drawn in Fig. 7 together with the results of the isotropic case. Figure 7 summarizes the results of the present work, e.g., shows the strain calibration curves obtained for the Si(100), (110), and (111) surfaces.

C. Silicon (111) surface

Figures 7 and 12 demonstrate that the Si(111) stripes under the application of strain along $[\bar{1}10]$ (configuration No. 8 in Table I) behave analogously to the above discussed Si(100) and Si(110) stripes under a [001] strain. The derivativelike structure at 3.39 eV and the broad band between 4 and 5 eV separated now into two bands are also present. In more recent RAS studies of strained (111) Si/SiO_2 interfaces,[25] the 3.4 eV resonance, that has been assigned to transitions at E_0' by Pollak and Cardona,[2] was assumed to be due to the combined contribution of both the E_0' and E_1 critical energies of Si. The RAS signal intensity increases linearly with increasing strain (Fig. 7) and is, within the experimental error, zero at zero strain. By comparison of the experimental RAS spectra [Fig. 13(a)] with the spectra calculated using Eqs. (4) and (11b) from the piezo-optical tensor components[17] [Fig. 13(b)], the bands at 3.39 and 4.34 eV (developing as RAS peak of opposite sign to the 4–5 eV band) are reproduced, but they are shifted to lower energies [as has been also observed in the case of the Si(100) and the Si(110) surfaces].

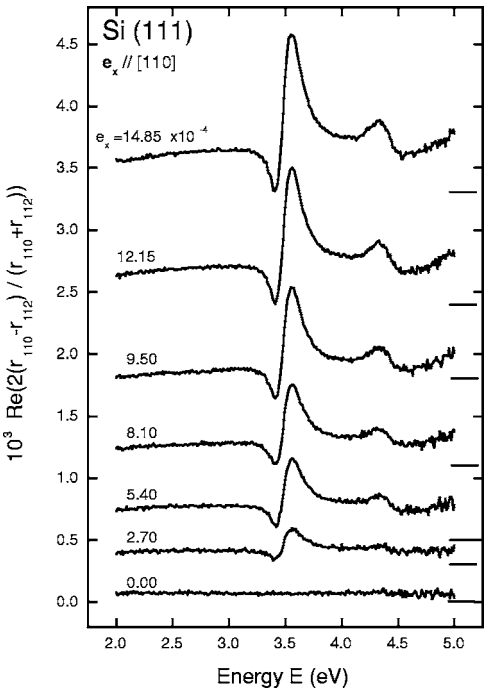

FIG. 12. Spectra of reflectance anisotropy ($r_{\bar{1}10}-r_{11\bar{2}}$) of Si(111) stripes strained along $[\bar{1}10]$ (for clarity, spectra are shifted in $\Delta r/\bar{r}$; zero strain lines are indicated).

CONCLUSIONS

According to our study, the sharp resonances induced by the stress in the reflectance anisotropy spectra of the silicon surface can be explained quantitatively as originating from the piezo-optical effect. Furthermore, it was demonstrated that Si (100), (110), and (111) surfaces exhibit under the application of strain along [011] or [001], or any other to these equivalent directions, changes in electronic band structure leading to the appearance of a derivativelike structure at a E_0' gap energy of 3.4 eV (Fig. 14). This feature is highly sensitive to the applied strain and increases linearly with strain magnitude (Fig. 7) making possible the detection of strains down to 10^{-5}. This is almost two orders of magnitude better than that achieved by other optical methods such as

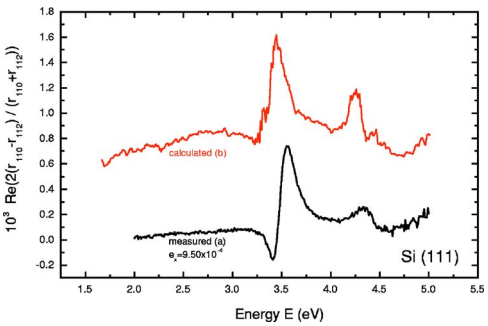

FIG. 13. (Color online) Comparison between (a) the experimentally measured reflectance anisotropy ($r_{\bar{1}10}-r_{11\bar{2}}$) of the Si(111) surface strained along $[\bar{1}10]$ and (b) the reflectance anisotropy calculated from the piezo-optical tensor components (Ref. 17) according to Eqs. (4) and (11b).

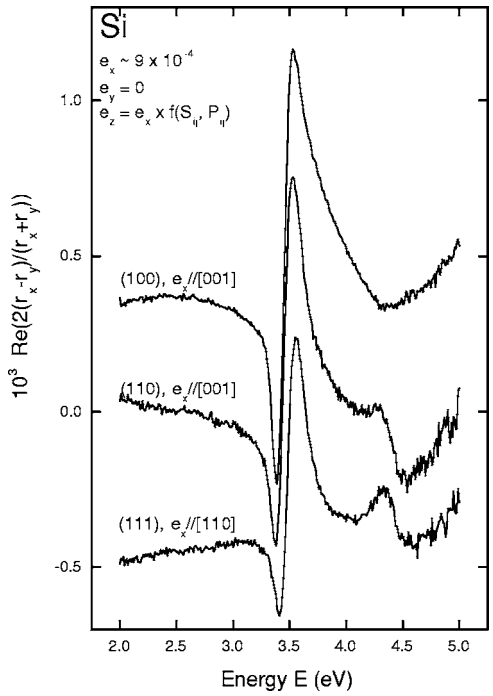

FIG. 14. Comparison of the 3.4 eV resonance at E_0'-gap energy in the reflectance anisotropy spectra of the silicon (100), (110), and (111) surfaces strained along low index crystallographic axes. The e_z strain can be estimated in dependence of the e_x strain, the elastic compliances S_{ij}, and the piezo-optical tensor P_{ij}.

Raman or PERS. We conclude, therefore, that strain-calibrated RAS data can be used efficiently to quantitatively measure very small amounts of strains such as those developing during semiconductor growth in lattice-mismatched heterostructures or by surface reconstruction and dimerization.

ACKNOWLEDGMENTS

Professor M. Cardona and Dr. P. Etchegoin are greatly acknowledged for their advice to the calculations involving the piezo-optical tensor. Acknowledged are also I. Gründler for the preparation of the Si stripes used and M. Wahl for his help with the drawings.

APPENDIX

The appendix summarizes the equantions that are necessary to evaluate the strain in the configurations used (Table I).

Determination of stress from measured strain. The stress-X_j and the strain-e_i optical tensors are related through the fourth rank elastic compliance S_{ij} (or elastic stiffness c_{ji}) tensors[15] according to

$$e_i = S_{ij} X_j. \tag{A1}$$

For cubic symmetric materials, the strain components along the principal axis $(x,y,z)=([100],[010],[001])$ are, in general, expressed in dependence of the applied stress as

$$e_x = S_{11}X_x + S_{12}X_y + S_{12}X_z,$$

$$e_y = S_{12}X_x + S_{11}X_y + S_{12}X_z,$$

$$e_z = S_{12}X_x + S_{12}X_y + S_{11}X_z,$$

$$e_{xy} = e_{xz} = e_{yx} = e_{yz} = e_{zx} = e_{zy} = 0. \tag{A2}$$

In case of a stress distribution in the x-y plane (biaxial stress), the stress component along the z axis is zero, $X_z=0$, and Eq. (A2) may be rewritten as

$$e_x = S_{11}X_x + S_{12}X_y,$$

$$e_y = S_{12}X_x + S_{11}X_y,$$

$$e_z = S_{12}(X_x + X_y). \tag{A3}$$

Under the assumption that there is no stripe deformation along the strain generating edge (Fig. 2), which means that $e_y=0$, Eq. (A3) yields

$$e_x = X_x\left(\frac{S_{11}^2 - S_{12}^2}{S_{11}}\right),$$

$$e_y = 0,$$

$$e_z = X_x S_{12}\left(\frac{S_{11} - S_{12}}{S_{11}}\right). \tag{A4}$$

Elimination of X_x in e_z leads to

$$e_z = e_x\left(\frac{S_{12}}{S_{11} + S_{12}}\right). \tag{A5}$$

The corresponding stress, given by using the elastic compliances, is then

$$X_x = e_x \frac{S_{11}}{S_{11}^2 - S_{12}^2},$$

$$X_y = -\frac{S_{12}}{S_{11}}X_x = -e_x\frac{S_{12}}{S_{11}^2 - S_{12}^2},$$

$$X_z = 0. \tag{A6}$$

As can be seen [Eq. (A4)], from the strain components, only the one parallel to the long side of the bent stripe (e_x) and the one normal to the stripe surface (in the direction z of the applied force e_z) are different from zero.[10] The first can be obtained, according to Eq. (2), in dependence of the stripe dimensions and the central deformation, while the latter can be calculated in terms of the strain component along the long side x of the stripe [Eq. (A5)]. Taking in account that the elastic properties of a crystal are different along different crystallographic directions, the strain components for all other configurations listed in Table I were derived after transformation of the elastic compliances in the respective configuration. This was achieved by applying a simplified method described in Ref. 20 for transforming fourth-rank

tensor properties of cubic crystals from the system of crystallographic axes $S(x,y,z)$ to any orthogonal system $S'(x',y',z')$. For the shake of clarity, this method will be briefly illustrated.

For tensors such as the elastic compliance (S-type tensors[15]), the components in S are defined, in suppressed index notation,[15] as follows: $S_{ij}=4S_{\lambda\mu\nu\rho}$ for i and $j=4$ to 6, $S_{ij}=2S_{\lambda\mu\nu\rho}$ for i or $j=4$ to 6, $S_{ij}=S_{\lambda\mu\nu\rho}$ otherwise. Transforming S_{ij} from S to S′ requires the 3×3 transformation matrix of the direction cosines l_a, m_a, n_a, i.e.,

$$A=\begin{bmatrix} l_1 & m_1 & n_1 \\ l_2 & m_2 & n_2 \\ l_3 & m_3 & n_3 \end{bmatrix}$$

or, alternatively, a 6×6 matrix based on A. In the method presented in Ref. 20, the only calculation involved is to determine, by simple inspection of A, the components of a 6×6 fully symmetric matrix T defined by $T_{ij}=T_{\lambda\mu\nu\rho}=l_\lambda l_\mu l_\nu l_\rho+m_\lambda m_\mu m_\nu m_\rho+n_\lambda n_\mu n_\nu n_\rho$. $T_{\lambda\mu\nu\rho}$ is a fourth-rank tensor itself, obeying the orthonormality relations $\Sigma_{j=1}^{3}T_{ij}=\Sigma_{j=1}^{3}T_{ji}=1$ for $i=1$ to 3 and $=0$ for $i=4$ to 6. In the limiting case of no rotation, T_{ij} takes the trivial form

$$T_{ij}^{0}=\begin{pmatrix} 1 & 0 & 0 & 0 & 0 & 0 \\ 0 & 1 & 0 & 0 & 0 & 0 \\ 0 & 0 & 1 & 0 & 0 & 0 \\ 0 & 0 & 0 & 0 & 0 & 0 \\ 0 & 0 & 0 & 0 & 0 & 0 \\ 0 & 0 & 0 & 0 & 0 & 0 \end{pmatrix}.$$

In terms of T_{ij}^{0} and T_{ij}, the components of the elastic compliances S_{ij} and S'_{ij} relative to S and S', respectively, can be written as

$$S'_{ij}=S_{ij}+S(T_{ij}-T_{ij}^{0}), \tag{A7}$$

where $S=S_{11}-S_{12}-S_{44}/2$. This particularly simple method, which allows one to obtain any rotated component S'_{ij} in terms of the fixed quantities S_{ij}, S, T_{ij}^{0} and the only variable but easy-to-obtain component T_{ij}, was applied in the special case of the Si stripes for all configurations listed in Table I.

To summarize, for a (100) Si-surface with e_x//[010] or [001] Eqs. (2) and (A5) result in

$$e_x=e_0,$$

$$e_y=0,$$

$$e_z=e_0\left(\frac{S_{12}}{S_{11}+S_{12}}\right). \tag{A8}$$

Thus, for stripes strained under the conditions described by Eq. (2), e_x is measured experimentally, $e_y=0$, and e_z can be calculated in dependence of e_x and the elastic compliances of the material.

For Si(100) with e_x//[011] or $[0\bar{1}1]$, the e_z strain will be given by

$$e_z=e_0\left(\frac{2(S_{11}+S_{12})-S_{44}}{4(S_{11}+S_{12})}\right). \tag{A9}$$

Similar equations can be derived for all configurations studied, as follows.

Si(110), e_x//$[\bar{1}10]$:

$$e_z=e_0\left(\frac{4S_{12}}{2S_{11}+6S_{12}+S_{44}}\right). \tag{A10}$$

Si(110), e_x//[001]. The e_z-strain is also given by Eq. (A8).

Si(110), e_x//$[\bar{1}11]$:

$$e_z=e_0\left(\frac{2(S_{11}+2S_{12})-S_{44}}{4(S_{11}+2S_{12})+S_{44}}\right). \tag{A11}$$

Si(111), e_x//$[\bar{1}10]$:

$$e_z=e\left(\frac{2(S_{11}+2S_{12})+(6S_{12}-S_{44})}{8(S_{11}+2S_{12})+2S_{44}}\right). \tag{A12}$$

[1] E. Anastassakis, in *Light Scattering in Semiconductor Structures and Superlattices*, edited by D. J. Lockwood and J. F. Young (Plenum Press, New York, 1991), p. 173.
[2] F. H. Pollak and M. Cardona, Phys. Rev. **172**, 816 (1968).
[3] E. Anastassakis, A. Cantarero, and M. Cardona, Phys. Rev. B **41**, 7529 (1990).
[4] E. Liarokapis and W. Richter, Meas. Sci. Technol. **3**, 347 (1992).
[5] E. Liarokapis, D. Papadimitriou, J. Rumberg, and W. Richter, Phys. Status Solidi B **211**, 309 (1999).
[6] K. Hingerl, R. E. Balderas-Navarro, A. Bonanni, P. Tichopadek, and W. G. Schmidt, Appl. Surf. Sci. **175-176**, 769 (2001).
[7] W. G. Schmidt, F. Bechstedt, and J. Bernholc, Phys. Rev. B **63**, 045322 (2001).
[8] M. Grundmann, Ph.D. thesis, TU, Berlin, 1991.
[9] D. E. Aspnes, J. Vac. Sci. Technol. B **3**, 1498 (1985).
[10] S. P. Timoshenko and S. Woinowsky-Krieger, *Theory of Plates and Shells* (McGraw-Hill, New York, 1989).
[11] L. D. Landau and E. M. Lifshitz, *Theory of Elasticity* (Pergamon Press, New York, 1970).
[12] M. Cardona, *Modulation Spectroscopy* (Academic Press, New York, 1969).
[13] P. Etchegoin, J. Kircher, M. Cardona, and C. Grein, Phys. Rev. B **45**, 11 721 (1992).
[14] M. Cardona, D. Rönnow, and P. V. Santos, Thin Solid Films **313-314**, 10 (1998).
[15] J. F. Nye, *Physical Properties of Crystals* (Oxford University Press, Oxford, 1976).
[16] B. O. Seraphin and N. Bottka, Phys. Rev. **145**, 628 (1966).
[17] P. Etchegoin, J. Kircher, and M. Cardona, Phys. Rev. B **47**, 10 292 (1993).
[18] D. E. Aspnes, J. Vac. Sci. Technol. B **3**, 1138 (1985).
[19] D. E. Aspnes and A. A. Studna, Phys. Rev. B **27**, 985 (1983).

[20] E. Anastassakis and E. Liarokapis, Phys. Status Solidi B **149**, K1 (1988).
[21] R. M. Tromp, R. J. Hamers, and J. E. Demuth, Phys. Rev. Lett. **55**, 1303 (1985).
[22] F. H. Pollak, in *Semiconductors and Semimetals* (AT&T Bell Laboratories, New York, 1990), Vol. 32, p. 17.
[23] W. Richter, Philos. Trans. R. Soc. London, Ser. A **344**, 453 (1993).
[24] B. S. Mendoza, R. Del Sole, and A. I. Shkrebtii, Phys. Rev. B **57**, R12 709 (1998).
[25] Z. Yang, Y. H. Chen, Jacob Y. L. Ho, W. K. Liu, X. M. Fang, and P. J. McCann, Appl. Phys. Lett. **71**, 87 (1997).